THE JOURNAL OF BIOLOGICAL CHEMISTRY VOL. 284, NO. 9, pp. 5956–5967, February 27, 2009

Spatial Distribution of Protein Kinase A Activity during Cell Migration Is Mediated by A-kinase Anchoring Protein AKAP Lbc*

Received for publication, July 22, 2008, and in revised form, December 19, 2008 Published, JBC Papers in Press, December 23, 2008, DOI 10.1074/jbc.M805606200

Adriana A. Paulucci-Holthauzen[‡], Leoncio A. Vergara[§], Larry J. Bellot[‡], David Canton[¶], John D. Scott[¶1], and Kathleen L. O'Connor[‡‖2]

From the [‡]Sealy Center for Cancer Cell Biology and Departments of [‖]Surgery, and of [§]Neurosciences and Cell Biology, University of Texas Medical Branch, Galveston, Texas 77555 and the [¶]Howard Hughes Medical Institute, Department of Pharmacology, University of Washington, Seattle, Washington 98195

Protein kinase A (PKA) has been suggested to be spatially regulated in migrating cells due to its ability to control signaling events that are critical for polarized actin cytoskeletal dynamics. Here, using the fluorescence resonance energy transfer-based A-kinase activity reporter (AKAR1), we find that PKA activity gradients form with the strongest activity at the leading edge and are restricted to the basal surface in migrating cells. The existence of these gradients was confirmed using immunocytochemistry using phospho-PKA substrate antibodies. This observation holds true for carcinoma cells migrating randomly on laminin-1 or stimulated to migrate on collagen I with lysophosphatidic acid. Phosphodiesterase inhibition allows the formation of PKA activity gradients; however, these gradients are no longer polarized. PKA activity gradients are not detected when a non-phosphorylatable mutant of AKAR1 is used, if PKA activity is inhibited with H-89 or protein kinase inhibitor, or when PKA anchoring is perturbed. We further find that a specific A-kinase anchoring protein, AKAP-Lbc, is a major contributor to the formation of these gradients. In summary, our data show that PKA activity gradients are generated at the leading edge of migrating cells and provide additional insight into the mechanisms of PKA regulation of cell motility.

Cell motility is controlled by a complex network of signals that are initiated by binding to the extracellular matrix. Understanding the biochemical mechanisms that control cell migration is necessary for better comprehension of processes like wound healing, embryonic development, and angiogenesis as well as cancer metastasis (1). PKA[3] is an important regulator of cell signaling and various biological functions (2–4). Previous studies have shown that cell motility is delicately controlled by synthesis and breakdown of cAMP through its effects on PKA. PKA regulates key signaling events that are critical for actin cytoskeletal remodeling and cell polarization during migration, including control of the activation states of RhoA, Rac, cdc42, Pak, and c-Abl. For example, PKA is known to inhibit the activation of RhoA, whereas it is required for the activation of Rac1, two proteins that are spatially regulated during cell migration. Therefore, it has been suggested that PKA activity in migrating cells is spatially regulated (5–9). The mounting evidence for the formation of cAMP/PKA gradients and their influence over directed cell motility is compelling. To conclusively determine that PKA activity gradients exist, the visualization of these gradients in single cells is needed to determine the nature of gradients and the mechanisms governing how they are formed.

The compartmental action of cAMP was suggested over three decades ago (10, 11) and has hence been shown to mediate the precise spatiotemporal control of its effectors (12–15). Tight control of cAMP levels is governed by the coordinated actions of cyclic nucleotide phosphodiesterases (PDEs) and adenylyl cyclases. Gradients of cAMP and, thus, PKA activity are expected to exist in a cell. This idea is based, most simplistically, on the fact that cAMP is generated by membrane-bound adenylyl cyclases and broken down by cytosolic PDEs; that is, the two arms of cAMP metabolism are spatially separated. Further compartmentalization of PKA activity also occurs as a result of the anchoring of PKA and cAMP-specific PDEs to A-kinase anchoring proteins (AKAPs), which has been demonstrated in a variety of cell types (16, 17). The anchoring of PKA occurs typically through the binding of the type II regulatory (RII) subunits to AKAPs where the relative levels of PDE activity and cAMP generated regulate the regional activity of PKA. PKA anchoring, in addition to cAMP synthesis and degradation, is believed to control spatial signaling of PKA (14, 15). Until recently, we have lacked both the model systems and technology to adequately study the possibility that cAMP/PKA activity gradients exist. We and others (5–8) have established that polarization and migration of cells are dependent on cAMP synthesis and breakdown. Here, we sought to demonstrate the existence of cAMP/PKA gradients in single migrating cells using the fluorescence resonance energy transfer (FRET)-based PKA biosensor A-kinase activity reporter (AKAR1) and determine how signaling components that regulate PKA activity, including cAMP synthesis, PDEs, and PKA anchoring, affect the formation of these gradients.

* This work was supported, in whole or in part, by National Institutes of Health Grants R21-GM071928 and R01-CA109136. The costs of publication of this article were defrayed in part by the payment of page charges. This article must therefore be hereby marked "*advertisement*" in accordance with 18 U.S.C. Section 1734 solely to indicate this fact.

[1] Supported by National Institutes of Health Grant HL088366 and the Fondation Leducq Transatlantic Network.

[2] To whom correspondence should be addressed: Dept. of Surgery, University of Texas Medical Branch, 301 University Blvd., Galveston, TX 77555-0525. Tel.: 409-772-1852; Fax: 409-747-1938; E-mail: kloconno@utmb.edu.

[3] The abbreviations used are: PKA, protein kinase A; AKAP, A-kinase anchoring proteins; AKAR1, A-kinase activity reporter; FRET, fluorescence resonance energy transfer; Fc, sensitized acceptor emission or corrected FRET; PDE, phosphodiesterase; PKI, protein kinase inhibitor; RII, type II regulatory; NT, non-targeting; LPA, lysophosphatidic acid; PIPES, 1,4-piperazinediethanesulfonic acid; CFP, cyan fluorescent protein; YFP, yellow fluorescent protein; siRNA, small interfering RNA; IBMX, isobutylmethylxanthine.

EXPERIMENTAL PROCEDURES

Cell Transfection and Treatments—Clone A colon carcinoma cells were grown to 70% confluence in RPMI plus 10% fetal calf serum before transfection with AKAR1, a non-phosphorylatable (S475A) mutant of AKAR1 (courtesy of Dr. Jin Zhang, Department of Pharmacology, Johns Hopkins University) (18), pECFP only, or pEYFP (BD Biosciences) constructs (16 μg/10-cm dish) using Lipofectamine^{TM} 2000 reagent (Invitrogen). At 24 h post-transfection cells were detached by trypsinization and washed 3 times with RPMI medium containing 0.25 mg/ml bovine serum albumin. Cells (1×10^6 cells/ml) were treated for 30 min with either 1 mM IBMX, 25 μM forskolin, 15 μM H-89, or 20 μM myristoylated protein kinase inhibitor (PKI) or for 5 min with 5 μM stHt31 or stHt31P (negative control for stHt31) as indicated. Cells were then plated onto coverslips coated with laminin-1 (10 μg/ml) in the presence of drug for 55 min at 37 °C. Cells were then fixed for 20 min at room temperature with 4% paraformaldehyde, 10 mM PIPES, pH 6.8, 2 mM EGTA, 2 mM $MgCl_2$, 7% sucrose, 100 mM KCl, 50 mM NaF, and 10 mM sodium pyrophosphate. Coverslips were then mounted with MOWIOL mounting medium (Calbiochem). Cells with recombinant protein expression levels high enough to give good fluorescence signal in lamellae were chosen for analysis.

For experiments using MDA-MB-231 cells, cells were grown to 70% confluence, suspended by trypsinization, and plated onto collagen-coated coverslips in serum-free Dulbecco's modified Eagle's medium containing 0.25 mg/ml of bovine serum albumin for 2–3 h. Cells were then stimulated with 100 nM lysophosphatidic acid (LPA) for 15 min or left untreated before fixation.

FRET Image Collection—Images were obtained using a Zeiss LSM-510 META confocal microscope with a 63×, 1.4 numerical aperture oil immersion objective (Optical Imaging Laboratory, University of Texas Medical Branch). The images where collected using two lines of excitation (458 and 514 nm, argon ion laser) and two different channels of emission. The intensity of fluorescence of cyan fluorescent protein (CFP) after CFP excitation at 458 nm (donor signal, I_{DD}) was obtained using a 470–500-nm bandpass filter. The intensity of fluorescence of yellow fluorescent protein (YFP; acceptor signal, I_{AA}) after excitation of YFP at 514 nm and the fluorescence intensity of FRET signal (raw FRET signal, I_{DA}) after excitation at 458 nm were measured using a 530–570-nm filter. All images were collected using 4-frame Kallman-averaging with a pixel time of 1.60 μs, a pixel size of 90 × 90 nm (scan zoom of 2 and a frame size of 792 × 792 pixels), and an optical slice of 0.8 μm. Because of the cell to cell variability of AKAR1 expression levels, the detector gains and the amplifier offsets were adjusted as needed to maximize the range of signal for each channel; however, the ratios between the gains of the three channels were kept constant. For each imagining session, the same collection conditions were used for cells expressing AKAR1 constructs, YFP, or CFP.

Image Processing—Images were imported into Metamorph software (Molecular Devices, Downingtown, PA) for processing. Initially, background was subtracted from all images based on the signal of non-cellular regions, and a low-pass filter was applied using a 5 × 5 kernel to improve the signal-to-noise ratio (19). To obtain a corrected FRET image (Fc), we processed the raw FRET image (I_{DA}) to compensate for nonspecific signals in the FRET channel, such as channel cross-talk due to the spectral overlap between CFP and YFP, defined by the equation $Fc = I_{DA}\text{-}\mathbf{a}I_{AA}\text{-}\mathbf{d}I_{DD}$ (20–22), where **a** and **d** represent cross-talk correction coefficients. The Fc values were then divided by the acceptor emission after direct acceptor excitation (I_{AA}) yielding the normalized FRET index (Fc/YFP), as proposed by van Rheenen *et al.* (19), which permitted the acquisition of higher resolution images under the conditions used here. These calculations correct for nonspecific signals present in specified channels, normalize for expression of the reporter construct throughout the cell, and render a FRET index independent of laser fluctuations (23). The cross-talk coefficients (**a** and **d**) were calculated using images collected from cells expressing either CFP (donor) or YFP (acceptor) alone. Coefficient **a** was obtained from the ratio of I_{DA} over I_{AA} for acceptor-only samples, whereas the coefficient **d** was obtained from the ratio of I_{DA} over I_{DD} for donor-only samples. For each imaging session, averages of coefficients **a** and **d** were calculated from at least 25 non-saturated regions using at least two different cells and three different sets of gains (note that there was no significant difference noted between the coefficients calculated at the different gains provided that the ratio between the gain intensities for the individual channels was kept constant). The constants were then used to calculate sensitized emission of the Fc for images collected on the same day. The Fc values were then normalized to the local concentration of construct using acceptor emission and reported as a ratio (Fc/YFP) as reported previously (19). For each cell analyzed, the average pixel intensity of Fc/YFP signal *versus* distance in microns was plotted such that the last distance point represents the edge of the cell, which represents the FRET gradient. For experiments involving siRNA-treated cells, the slopes of multiple line scans were calculated, averaged, and reported in a histogram plot (untreated, $n = 20$; non-targeting siRNA, $n = 19$; AKAP-Lbc siRNA number 3, $n = 11$, and number 5, $n = 9$). The slopes were taken from the last 90 pixels (equivalent to 8 μm) of each line scan, where the gradients of Fc/YFP are consistently found in untreated cells. This approach was used to standardize the distance analyzed from the leading edge to the cell body and to avoid selection bias. For all data cells shown represent cells from at least two coverslips and a minimum of three separate experiments.

PKA Assays—Active PKA was assessed by pseudosubstrate affinity precipitation of cell lysates, as described (24). Briefly, cells were plated on laminin-coated dishes in the presence of select inhibitors and then harvested in a hypotonic buffer and gently sonicated. A portion of cleared lysates (1 part) was set aside as a loading control, and the remaining lysate (10 parts) was incubated with beads conjugated to glutathione *S*-transferase-PKI fusion protein for 30 min at 4 °C and then rinsed. Glutathione *S*-transferase-PKI (active)-bound PKA and lysate controls (10% total) were then immunoblotted for the PKA catalytic subunit (BD Transduction Laboratories). Several exposures were analyzed and quantified by digital capture of luminescence using a Fluorochem^{TM} 8900 luminescent imager

(Alpha Innotech) to ensure that signals remain in the linear range.

Small Interference RNA Treatment—Suspended cells (3×10^6) were electroporated with 16 μg of AKAR1 alone or in conjunction with 200 nM siRNA specific for AKAP-Lbc (AKAP13) or a control (non-targeting) sequence (Dharmacon, Inc.) as reported previously (25). Individual sequences for AKAP-Lbc are UCAACAGACUCACUAAAUAUU (number 3) and GGAAGAAGCUUGUACGUGAUU (number 5). Cells were then kept in normal growth medium for 48 h and then assessed for target gene expression using immunoblot analysis, PKA-FRET, or cell migration.

Immunoblotting—Cells were harvested using radioimmune precipitation assay buffer (150 mM NaCl, 0.5 mM EGTA, 0.5% sodium deoxycholate, 0.1% SDS, 1% Triton X-100, 50 mM Tris-HCl, pH 7.4) containing 15 μg/ml protease inhibitor mixture (Sigma Aldrich) and 1 mM phenylmethanesulfonyl fluoride. Total protein was then electrophoresed on a 7.5% SDS-PAGE and transferred to nitrocellulose. The membrane was cut, blocked with 5% nonfat dry milk, and then probed for either AKAP-Lbc (1:5000 dilution, rabbit polyclonal, VO-96, supplied by Dr. Ben Pedroja, Vollum Institute/OHSU) or β-tubulin (1:1000 dilution, rat monoclonal antibody 1864, Chemicon).

Migration Assays—For laminin haptotaxis assays the lower compartments of Transwell chambers (6.5-mm diameter, 8-μm pore size; Costar) were coated with 15 μg/ml laminin-1. Cells (1×10^5) suspended in RPMI/ bovine serum albumin were added to the upper chamber and incubated at 37 °C for 4 h. Cells were removed from the upper chamber with a cotton swab, and migrated cells on the lower membrane surface were fixed, stained with crystal violet, and quantified visually as described previously (26).

Immunocytochemistry—Cells were fixed for 10 min at room temperature with 4% paraformaldehyde, 10 mM PIPES, pH 6.8, 2 mM EGTA, 2 mM $MgCl_2$, 7% sucrose, 100 mM KCl, 50 mM NaF, and 10 mM sodium pyrophosphate, rinsed in phosphate-buffered saline (PBS) for 20 min, permeabilized with 0.5% Triton X-100 in PBS, and then rinsed. Cells were incubated in block solution (3% bovine serum albumin, 1% normal goat serum in phosphate-buffered saline) for 30 min and then incubated overnight with 1:100 dilution of phospho-PKA substrate (RR*X*S/T) monoclonal antibody (100G7, Cell Signaling Technologies) in block solution at 4 °C. After three 10-min phosphate-buffered saline washes, cells were incubated with either Alexa 594- or Alexa 488-conjugated secondary, rinsed, mounted with MOWIOL mounting medium (Calbiochem), and imaged by confocal microscopy.

Statistics—Pairwise comparisons between AKAR-transfected *versus* each of the non-targeting (NT) and siRNA groups were carried out using the two-sample *t* test. Normality and equal variance assumptions were assessed, and log transformation was employed as necessary before conduct of the parametric tests.

RESULTS

To determine the spatial distribution of PKA activity in migrating cells, we utilized the previously characterized AKAR1 single-molecule FRET sensor (18). AKAR1 contains a modified Kemptide sequence that can be phosphorylated by PKA and the phosphoamino acid binding domain of 14-3-3τ, which binds to this phosphorylated sequence. These domains are flanked by CFP and YFP that display FRET upon binding of the phosphorylated Kemptide sequence to the 14-3-3τ domain, thereby indicating where PKA is active. The FRET emitted by this construct is initiated by PKA and is likely terminated by an uncharacterized phosphatase. Thus, this signal represents the lifetime of phosphate for a single type of PKA substrate. As a cell model for assessing the nature of PKA activity gradients during migration, we utilize the cAMP-sensitive Clone A migration model. Clone A cells adhere to and migrate randomly on laminin-1 by signaling through the $\alpha 2\beta 1$ and $\alpha 6\beta 4$ integrins (27). Migrating Clone A cells form a polarized morphology in which the leading edge is marked with a ruffling lamellipodium. Time-lapse videomicroscopic analysis of these cells shows that cells migrate in a forward direction toward the lamellipodial ruffle. If multiple lamellipodia are present, one will eventually become dominant, and the cell will move in the direction of the new dominant lamellae (data not shown). Therefore, we are able to identify migrating cells by the presence of a lamellipodial ruffle which signifies the leading edge and retraction fibers at the trailing edge.

To determine the spatial distribution of cAMP/PKA activity, Clone A cells transfected with either AKAR1, a non-phosphorylatable mutant (S475A) of AKAR1, CFP-only, or YFP-only constructs were allowed to migrate on laminin-1 and then fixed. Lamellar area quantification of cells transfected with AKAR1 and untreated cells notably shows that cells expressing the AKAR1 construct display no differences in morphology when compared with untreated cells (n for each condition equals 20; data not shown). Cells expressing levels of construct sufficient for good resolution of fluorescent signal in the lamellar region were then imaged using a confocal microscope with a three-filter set for the determination of sensitized acceptor emission or corrected FRET (Fc) (20, 21), as detailed under "Experimental Procedures." Correction coefficients for bleed-through were calculated from cells transfected with CFP or YFP alone. This method of obtaining FRET values has been proven to generate high resolution images (20, 28) that are independent of the photoconversion of YFP into CFP-like species that occurs during acceptor photobleaching experiments (29). The Fc value was then normalized to the local concentration of construct and reported as a ratio with acceptor emissions (Fc/YFP) as previously suggested (19), permitting a more accurate readout for PKA activity. Under wide-field optics, the larger volume and, thus, higher fluorescence within the cell body caused light scattering that prevented definition of cell borders and lamellar structures. Therefore, confocal analysis was necessary to obtain proper resolution. As shown in Fig. 1*A*, Clone A cells induced to migrate on laminin-1 show a higher Fc/YFP signal within lamellae with a marked gradient of increasing intensity culminating at the leading edge, indicating higher PKA activity in this region and the presence of a gradient of PKA activity (representative of 14 of 15 cells imaged). Further analysis of line scans within the image show graphically that the Fc/YFP ratio increases dramatically in the lamellae area, demonstrating that PKA activity is spatially distributed within the cell during migration.

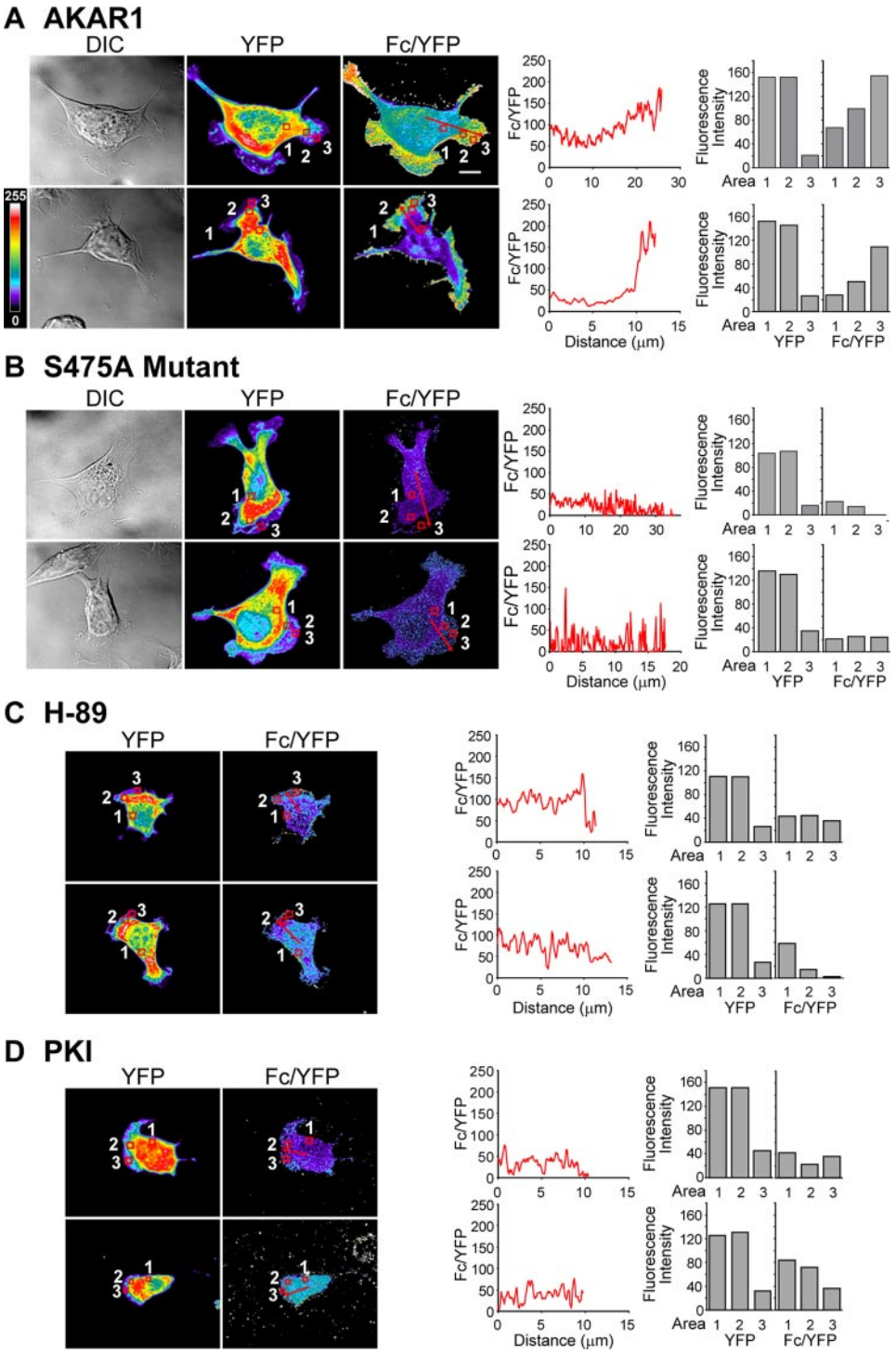

FIGURE 1. **PKA is spatially activated in Clone A cells.** Clone A cells transiently transfected with AKAR1 (*A*) or S475 AKAR1 mutant (*B*) were plated onto laminin-coated coverslips and allowed to migrate before fixation and imaging. Alternatively, AKAR1-expressing cells were treated with 15 μM H-89 (*C*) or 20 μM PKI (*D*) and plated on laminin-1 in the presence of indicated drug. Representative images taken at the base of the cell by confocal microscopy depicting differential interference contrast (*DIC*, *left*), YFP (*middle*), and Fc/YFP (*right*) are shown for two separate cells. YFP and Fc/YFP intensities are represented by pseudocolor; the scale is indicated at the *left side* of the figure of the Fc/YFP *panels* in *A*. *Line graphics to the right* of the Fc/YFP images represent the average pixel intensity of the Fc/YFP ratio (on a scale of 0–255) *versus* the distance in microns marked by the *red line scan* in the corresponding images. *Bar graphics* represent fluorescence intensity for YFP and Fc/YFP for regions noted by the *red boxes* in the YFP and Fc/YFP panels, respectively. The *bar* in the upper Fc/YFP panel of *A* indicates 10 μm and is representative of the scale for all images.

To confirm that the observed gradients in Fc/YFP signal are specific to PKA activity and not a result of cell processing, image handling, or phosphorylation of AKAR1 from another kinase, several controls were performed. Initially, cells were transfected with the S475A mutant of AKAR1 that cannot be phosphorylated by PKA and, therefore, should not emit FRET as demonstrated previously (18). Cells plated on laminin-1 that were chosen for analysis were morphologically similar to those expressing the AKAR1 construct and were processed in an identical manner. In Fig. 1*B* we show that cells expressing the S475A mutant construct displayed very low FRET and were devoid of any apparent gradient in the residual signal, as shown by the Fc/YFP panels (representative of 7 of 7 cells analyzed) and line scan graphics and region analysis. Next, we sought to confirm that the FRET signal observed was specific and a direct result of PKA activity. For these experiments we treated AKAR1-expressing cells with PKA-specific inhibitors, H-89, and the naturally occurring PKI before and during migration on laminin-1. Clone A cells are unique in the fact that they continue to form lamellae and membrane ruffles under conditions in which PKA is inhibited, as they utilize RhoA for these processes and not Rac1 (26), which requires PKA activity to function (6, 7, 30). Therefore, the contributions of PKA to the FRET signal in AKAR1-expressing cells can still be monitored in lamellar structures. Here, we find that cells treated with H-89 (Fig. 1*C*; representative of 10–12 cells imaged) or PKI (Fig. 1*D*; representative of 7 of 9 cells imaged) show minimal FRET and no PKA activity gradients similar to cells expressing the S475A AKAR1 mutant.

Notably, the PKA activity gradients are present predominantly in the lamellae (~0.1 μm in thickness) where the cell volume is less than the optical sections taken within the cell body (0.8 μm thick). To confirm that our results are not a consequence of changes in the intracellular concentration of AKAR1 or the shallow depth at the periphery, we performed region analysis of cells. Regions 1 and 2 where chosen to contain similar YFP intensities where region 1 is present in the cell body and region

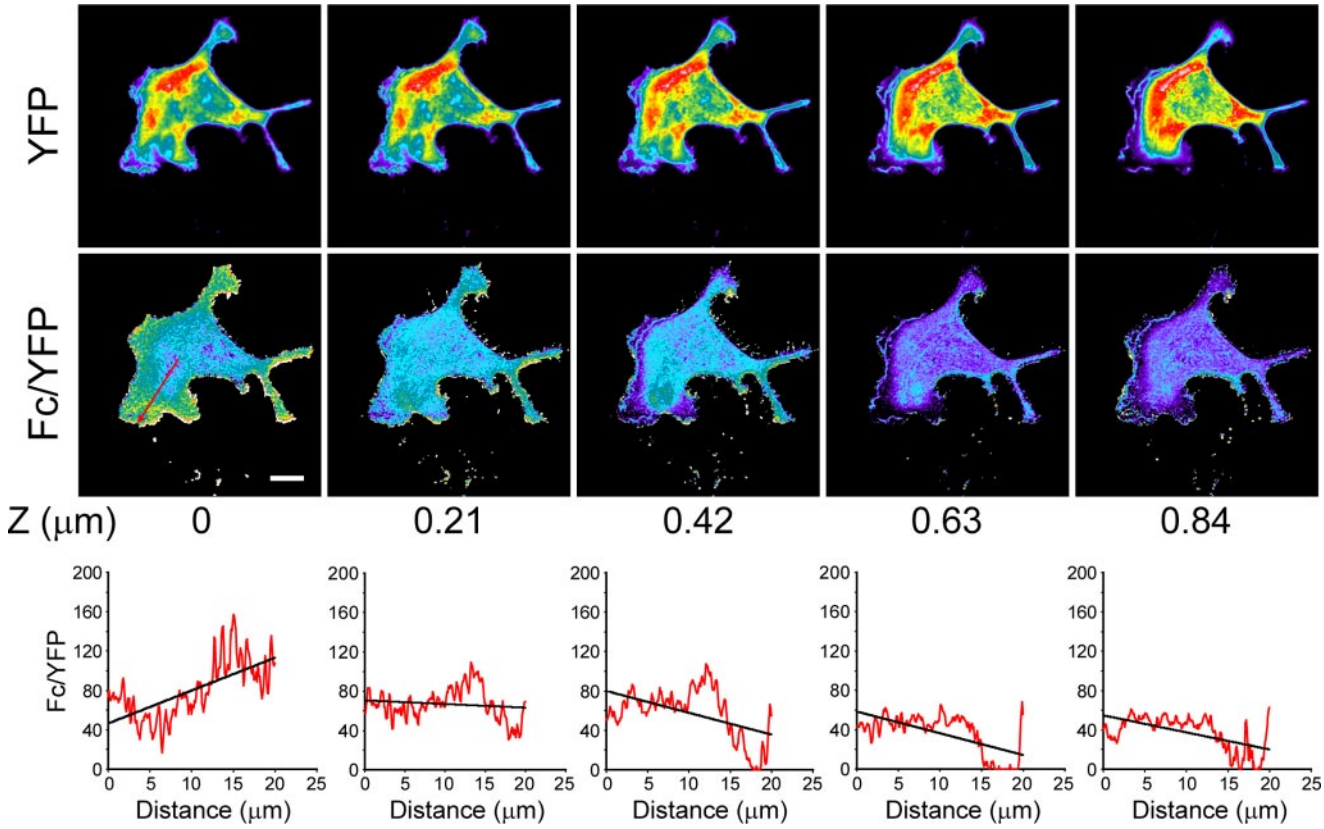

FIGURE 2. **PKA gradients are restricted to the basal surface of the cell.** Cells expressing AKAR1 were treated as in Fig. 1*A* and analyzed for FRET over several planes along the *z* axis at an interval of 0.21 μm. Note that the PKA gradient is seen only in the most basal portion of the cell. Graphics represent the average pixel intensity of the Fc/YFP ratio *versus* the distance in microns as displayed in Fig. 1. The *bar* in the left-hand Fc/YFP indicates 10 μm.

2 is found near the leading edge. Region 3 was chosen at the leading edge and contains the same area as regions 1 and 2. As shown in the histograms in Fig. 1*A*, we observe that region 2 contains an increased average Fc/YFP intensity compared with region 1 in untreated cells. Region 3 in these cells displays even higher Fc/YFP intensity, thus confirming the presence of a gradient. In contrast, the S475 construct-transfected cells or H89 or PKI-treated cells show no change or a decrease in FRET intensity between regions. Collectively, these data confirm that the FRET signal detected with AKAR1 in migrating cells is specifically due to the PKA phosphorylation of the AKAR1 construct and is in agreement with the specificity demonstrated by the original characterization of AKAR1 (18).

To determine whether PKA activity gradients exist vertically within the lamellipodium, we analyzed serial confocal sections of migrating Clone A cells expressing the AKAR1 construct at 0.2-μm intervals. As depicted in Fig. 2, the gradients are found primarily within the basal most section. These data demonstrate that the PKA activity gradients are tightly associated with the basal plasma membrane within close proximity to the regions where new integrin contacts are being made during the migratory process. These observations suggest that cAMP/activated PKA gradients form dorsal-ventrally within the lamellipodium as well as from the leading edge-rearward.

Next we sought to determine which signaling components known to regulate cAMP signaling are involved in the formation of these PKA activity gradients. Tissue-specific expression and compartmentalization of PDEs are expected to control cAMP gradients in all cell types and influence the integration of signaling pathways (31). Importantly, PDE activity has been previously shown to be important for cell motility (5, 26, 32). To investigate how PDEs influence cAMP gradient formation, AKAR1-expressing Clone A cells were treated with the broad spectrum PDE inhibitor IBMX, plated on laminin-1, fixed, and submitted to confocal analysis to determine FRET. As shown in Fig. 3*A*, we find that cells treated with IBMX (11 of 11 cells analyzed) also display PKA activity gradients as indicated by the high Fc/YFP intensity within cellular protrusions compared with the body of the cell. Linescan and region analyses of the Fc/YFP ratio (Fig. 3*A*, *lower panels*) reveal that the degree of the PKA gradient is comparable with untreated cells. However, cells no longer display a polarized distribution of PKA activity; that is, the gradient is not restricted to a single side or leading edge but is found all along the periphery of the cell (compare Fig. 1*A* to 3*A*). This observation is in accordance with a loss of cell polarization and subsequent reduction in directed cell motility that has previously been reported by PDE inhibition (5, 26, 32).

The normalized FRET index or the apparent FRET efficiency (Fc/YFP) is not a direct measurement of the FRET efficiency and, therefore, can only be used to determine how differences in activity are distributed within a cell. For this reason we measured the total PKA activity levels in cells utilizing a pseudosubstrate affinity precipitation assay that was recently developed to assay active PKA. This assay is based on the ability of an active kinase to bind a pseudosubstrate such as that found in the nat-

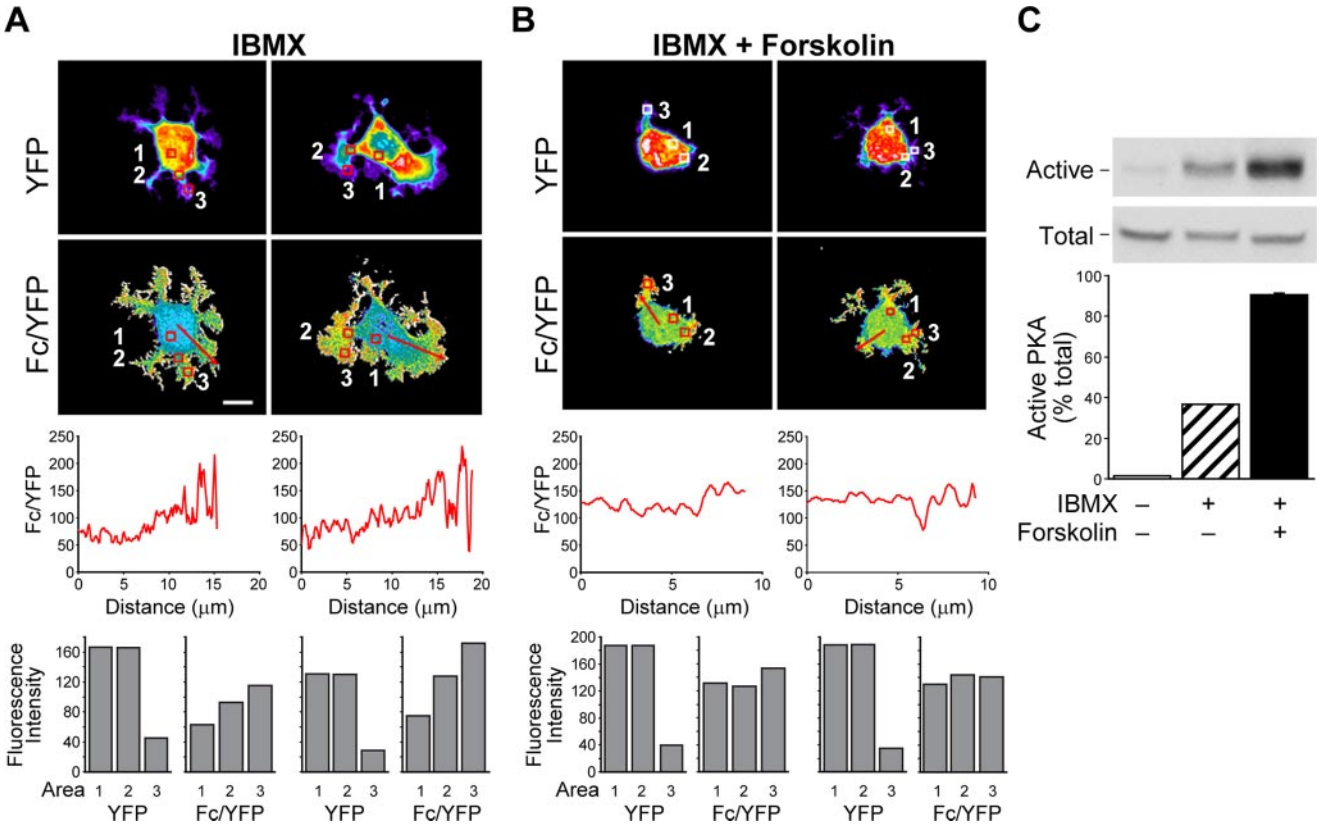

FIGURE 3. **Inhibition of PDE activity and activation of adenylyl cyclases increase PKA activity levels, disrupt cell polarization, and alter the gradients of PKA activity.** Clone A cells were treated with 1 mM IBMX (*A*) or 1 mM IBMX plus 25 μM forskolin (*B*) and plated on laminin-1-coated coverslips in the presence of the same concentrations of drugs and imaged as described in Fig. 1. *Line graphics below* the Fc/YFP images represent the average pixel intensity of the Fc/YFP ratio *versus* the distance in microns. *Bar graphics* represent fluorescence intensity for YFP and Fc/YFP for regions noted by the *red boxes* as displayed in Fig. 1. The *bar* in the *left-hand Fc/YFP panel* of *A* indicates 10 μm and is representative of the scale for all images. *C*, Clone A cells treated with 1 mM IBMX or 1 mM IBMX plus 25 μM forskolin or left untreated were plated on laminin-1-coated dishes for 30 min then extracted, and active PKA levels relative to total PKA were measured using a pseudosubstrate affinity assay. Glutathione *S*-transferase-PKI bound PKA (*Active*) and lysate controls (*Total*, representing 10% input) were immunoblotted for the PKA catalytic subunit and then quantified (*graphs*). Note that immunoblots are from the same gel, same exposure. Representative data are shown.

urally occurring PKA inhibitor PKI. The pseudosubstrate region of PKI contains a serine to alanine substitution in the PKA consensus phosphorylation site; therefore, it binds the PKA active site with high affinity. With this assay, we use a fusion protein which contains the PKI pseudosubstrate domain peptide fused to glutathione *S*-transferase and bound to glutathione beads to precipitate out active PKA from cell lysates and give a read-out of the percentage of active kinase found within the cell population. The principle of this assay has been validated and found to be more sensitive than traditional radioactivity-based kinase assays (24). Using the pseudosubstrate affinity assay, we find that ~40% of the total PKA is active when cells are treated with the PDE inhibitor IBMX (Fig. 3*C*). Because increases in cAMP resulting from PDE inhibition and subsequently PKA activation are reliant on basal cAMP synthesis (14, 15), we used co-stimulation with forskolin to achieve full activation of PKA (Fig. 3*C*). In cells co-stimulated with IBMX and forskolin, PKA activity gradients were completely disrupted (representative of 7 of 8 cells imaged), as shown by line scan and by region analysis, and cell spreading and polarization were dramatically altered (Fig. 3*B*). These data suggest that the PKA activity gradients may exist as a result of limited diffusion of cAMP after synthesis rather than the spatial distribution of the PKA catalytic subunits themselves.

To confirm that our FRET data are representative of other PKA substrates, we turned to immunohistochemistry using phospho-PKA substrate-specific antibodies as has been described previously (33). For these experiments Clone A cells were left untreated or pretreated with H-89, IBMX, or IBMX plus forskolin before plating on laminin-coated coverslips and then immunostained with phospho-PKA substrate-specific antibodies. As shown in Fig. 4, H-89 treatment reduces, although does not completely eliminate, immunostaining for the phospho-PKA substrate, whereas IBMX and IBMX plus forskolin treatment dramatically enhances immunoreactivity. These observations are quantified using regional analysis comparing staining intensity of the cell body (region 1) to that of the periphery (region 2). These controls demonstrate that the staining with phospho-PKA substrate antibody changes appropriately with conditions that alter PKA activity. In the untreated cells we find substantial immunoreactivity in the lamellae, although it appears less intense than the cell body. However, even under confocal conditions, the section of the cell body imaged is substantially thicker than the lamellae. This is evidenced by the ~7-fold differences in YFP intensity between the lamellae and cell body (Fig. 1*A*, *bar graphics*). These observations suggest that the total phospho-PKA substrate concentration of the lamellae is higher per unit cytosol than that of the cell body.

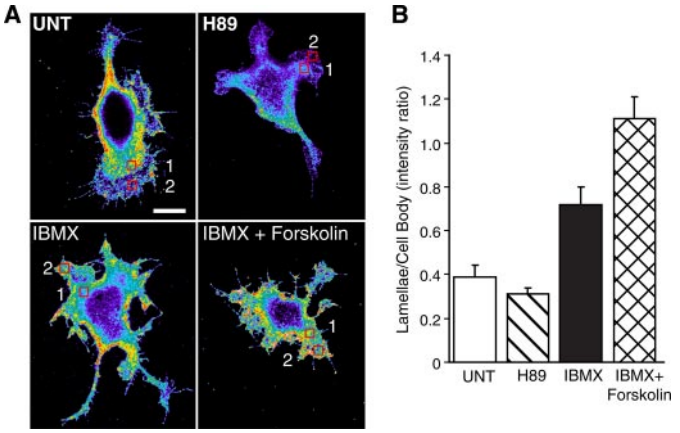

FIGURE 4. **Immunocytochemistry for phospho-PKA substrates.** *A*, Clone A cells were left untreated (*UNT*) or pretreated with 15 μM H89, 1 mM IBMX, or 1 mM IBMX plus 25 μM forskolin and then plated on laminin-1-coated coverslips in the presence of drug. After 45 min cells were fixed and then immunostained for phospho-PKA substrates as described under "Experimental Procedures." Cells were then imaged by confocal microscopy under the same conditions including the gain and exposure times. Cells shown here were imaged on the same day. The *bar* in the untreated panel indicates 10 μm and is representative of the scale for all images. *B*, regional analysis was performed to compare immunostaining intensity between each condition. Graphics represent the average ratio of intensity of an area taken at the leading edge of the cell (region 2) relative to an area in the cell body (region 1) from 10 different cells from at least two different coverslips. *Error bars* represent S.E.

Recently, Howe *et al.* (7) showed that PKA activity and RII subunits accumulate in pseudopodial extensions of growth factor-stimulated fibroblasts. Furthermore, they show that this accumulation is dependent upon PKA anchoring proteins. To determine whether PKA anchoring is instrumental in the formation of PKA activity gradients, we utilize stearated peptide stHt31, which perturbs RII subunit binding to AKAPs and prevents PKA anchoring, and the control peptide stHt31P, which differs in sequence from the stHT31 peptide by two isoleucine to proline substitutions (34). As shown in Fig. 5*A*, the stHt31P control peptide does not inhibit cell polarization and maintains the PKA activity gradients observed for untreated cells (observed in 6 of 6 cells imaged). However, stHt31 anchoring inhibitor peptide effectively blocks the formation of cell protrusions and prevents the formation of PKA activity gradients (Fig. 5*B*; (representative of 7 of 9 cells imaged). Importantly, treatment of cells with these peptides does not significantly alter overall cellular PKA activity levels, as shown in Fig. 5*C*, but rather its distribution. These data strongly suggest that cAMP accumulation coupled with PKA anchoring is responsible for the generation of PKA gradients.

Next, we sought to determine which AKAPs may be involved in PKA activity gradient formation. Because of the localization

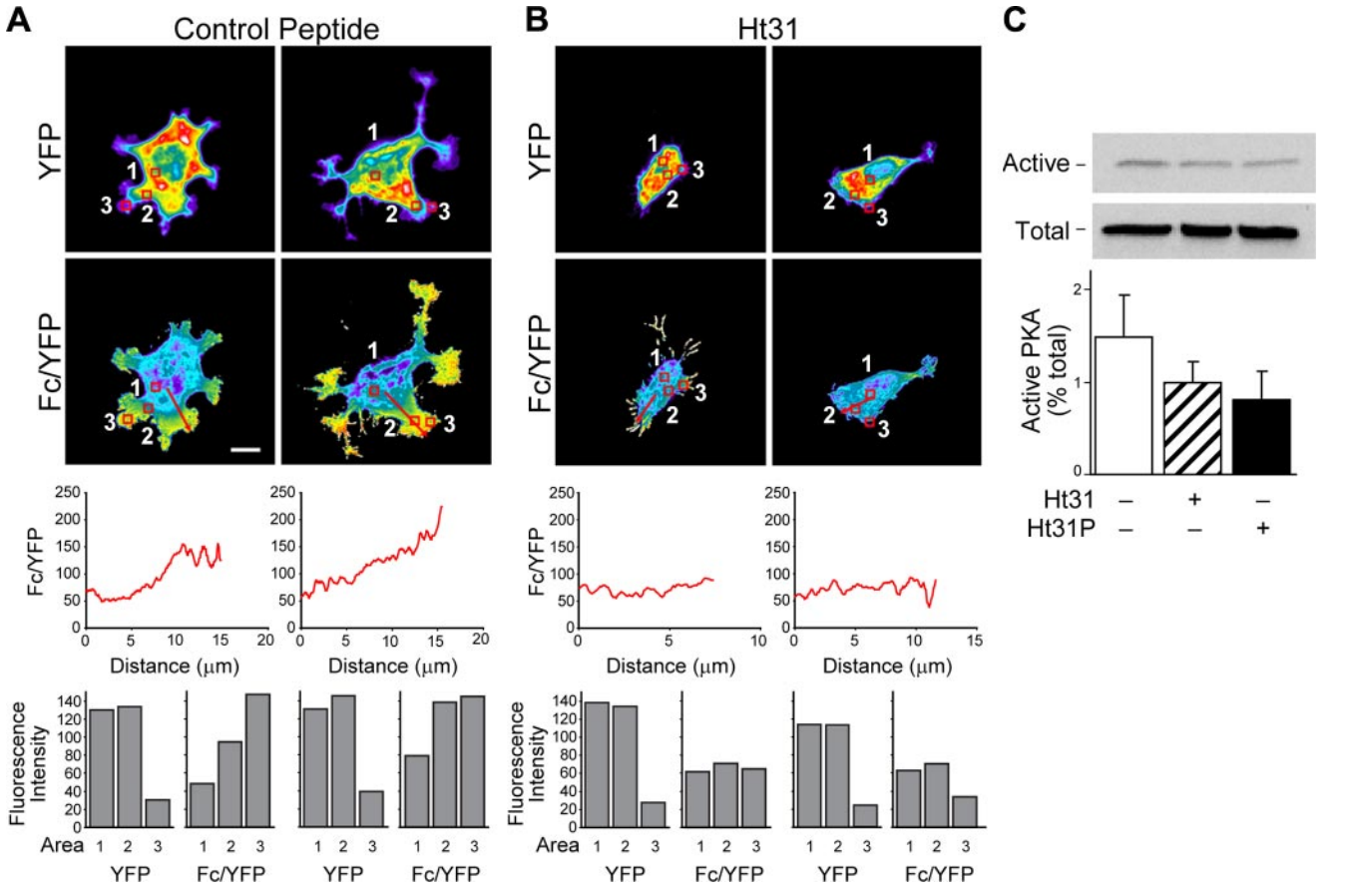

FIGURE 5. **Anchorage of PKA is crucial for cell polarization and gradients of active PKA.** Clone A cells were incubated with 5 μM stHt31P control peptide (*A*) or stHt31 (*B*) and then plated on laminin-1-coated coverslips and allowed to adhere and migrate in the presence of peptide. Cells and images were processed as described in Fig. 1. Graphics below the Fc/YFP images represent the average pixel intensity of the Fc/YFP ratio *versus* the distance in microns as displayed in Fig. 1. *Bar graphics* represent fluorescence intensity for YFP and Fc/YFP for regions noted by the *red boxes*. The *bar* in the left-hand Fc/YFP panel of *A* indicates 10 μm and is representative of the scale for all images. *C*, Clone A cells were incubated with 5 μM stHt31P control peptide or 5 μM stHt31 or left untreated and then plated onto laminin-1-coated 100-mm dishes for 50 min. Cells were then extracted, and active PKA was measured as described in Fig. 3. Representative data are shown.

of these gradients close to the basal plasma membrane and the effects of PKA on the actin cytoskeleton, we focused our attentions on plasma membrane and actin cytoskeletal-associated AKAPs. Using RII overlay methodology and immunoblot analysis, we find that Gravin and AKAP-KL are not expressed in Clone A cells, but AKAP-Lbc, Yotiao, and Ezrin are present (data not shown). Because Yotiao is associated with specific ion channels (14, 35, 36) and Ezrin is preferentially associated with membrane ruffles (37), we focused our attentions on the actin cytoskeleton-associated AKAP-Lbc. AKAP-Lbc is a 312-kDa protein which functions as a guanine nucleotide exchange factor for RhoA downstream of lysophosphatidic acid (38). Notably, the Ht31 peptide used to disrupt PKA anchoring is derived from the RII subunit binding domain of AKAP-Lbc (34). For these experiments we used empirically determined individual siRNAs to silence the expression of AKAP-Lbc. With successful suppression of AKAP-Lbc, we plated Clone A cells on laminin, stained cells with TRITC-phalloidin, and quantified lamellar area as previously reported (26). Untreated cells, cells treated with NT siRNA, and cells treated either with AKAP Lbc siRNA 3 or AKAP-Lbc siRNA 5 spread similarly and presented with comparable lamellar area (data not shown).

Clone A cells were then co-transfected with the AKAR1 construct and either NT siRNA or the individual AKAP-Lbc siRNAs and compared with cells transfected with AKAR1 alone. FRET analysis reveals that AKAR1 only and AKAR1 plus NT siRNA-transfected cells display strong PKA activity gradients at the leading edge of the cell (Fig. 6*A*, *left panels*). The FRET efficiency (Fc/YFP) observed along a representative arrow traced inside the cell is graphically represented below the respective cell image. Cells treated with individual AKAP-Lbc siRNAs, in contrast, showed substantially less PKA activity within the lamellae, as evidenced by the reduced slope of the FRET efficiency *versus* distance curve when compared with the controls (Fig. 6*A*, *right panels*). Silencing of AKAP-Lbc expression was confirmed by immunoblot analysis (Fig. 6*B*). To verify that the decrease in gradient observed is representative, we calculated the average slope of the Fc/YFP *versus* distance curve using multiple cells under each condition. As depicted in the histogram plot (Fig. 6*C*), the average slope for untreated ($n = 20$) and NT siRNA-treated ($n = 19$) cells are 0.55 and 0.50, respectively, whereas for AKAP Lbc siRNA 3 ($n = 11$) or AKAP-Lbc siRNA 5 ($n = 9$)-treated cells they are, respectively, 0.23 and 0.20. Similar results were obtained using the Dharmacon siRNA SMARTPool ($n = 22$), which yielded a slope of 0.22 (data not shown). Collectively, these data demonstrate that AKAP-Lbc contributes substantially to the formation of PKA activity gradients.

Next we sought to determine how the silencing of AKAP-Lbc expression affects cell migration. For these experiments, control and siRNA-treated cells were subjected to haptotactic migration on laminin-1. As shown in Fig. 6*D*, a significant decrease (30–40%) in migration was observed with the siRNA-mediated reduction of AKAP-Lbc expression. These data are in accordance with the observation that AKAP-Lbc ablation diminished, but does not abolish, the formation of PKA activity gradients for cells migrating on laminin.

To confirm that the existence of PKA activity gradients exists in other cell types undergoing different forms of migration, we analyzed MDA-MB-231 cells stimulated with LPA. MDA-MB-231 breast carcinoma cells migrate efficiently toward LPA (39). Their chemotactic migration toward LPA is inhibited by both PKA and PDE inhibition using H-89 or PKI and IBMX, respectively (data not shown). To determine whether PKA activity gradients also exist in these cells, cells were left untreated or stimulated with 100 nM LPA for 15 min. Unlike untreated cells, LPA-stimulated MDA-MB-231 cells showed a high concentration of phospho-PKA substrate at the leading edge compared with the cell body (Fig. 7). Together, these data suggest that PKA activity gradients exist in migrating cells and are properly positioned to influence signaling events at the leading edge of migrating cells.

DISCUSSION

Previous studies have suggested that PKA activity can either facilitate or inhibit actin cytoskeletal organization and cell migration. This pleiotropic role of PKA suggests a significant degree of complexity for regulation of PKA activity during cell migration. We and others (6–9) have suggested that PKA activity gradients exist in migrating cells to facilitate polarization of cells and proper spatial signaling for the organization of distinct actin cytoskeletal structures. The first solid evidence that PKA activity is compartmentalized in migrating cells came from Howe *et al.* (7). They demonstrated a polarized enrichment of PKA regulatory subunits and activity to the protrusive, lamellipodial structures formed during fibroblast chemotactic migration. This enrichment of RIIα and PKA activity correlated with an increased level of phosphorylation of the PKA substrates VASP and PTP-PEST. Our data conclusively demonstrate the existence of PKA activity gradients in single migrating cells and that these gradients are properly localized to influence key regulators of actin cytoskeletal reorganization within the lamellae. Furthermore, we find that these gradients are found in close proximity to where integrins interact with the extracellular matrix. These data are in accordance with recent findings using a membrane-targeted pmAKAR3 construct that PKA activity is highest at the leading edge in cells migrating on a fibronectin substrata using $\alpha4\beta1$ and $\alpha5\beta1$ integrins (33). Combined with our work where we use laminin and collagen matrices, these observations suggest a universal integrin involvement in the formation of PKA activity gradients. Importantly, integrin extracellular matrix receptors have been implicated in control of cAMP and PKA through the activation of PDEs (5), stimulation of cAMP synthesis (40), and association with PKA anchoring (41). Our study further clarifies how the PKA activity compartmentalization and gradient are mediated in migrating cells. In total, our data suggest that PKA anchoring coupled with cAMP synthesis and limited diffusion of cAMP is responsible for the generation of PKA gradients, whereas PDE activity restricts the formation of the gradient to the leading edge within migrating cells.

Although the role of AKAPs in cell migration has been conceptually linked, how specific AKAPs contribute to cell migration is not well understood. Importantly, we find that a single AKAP, namely AKAP-Lbc, can play a substantial role in the formation of PKA activity gradients and, ultimately, cell migration. Previous studies on AKAP-Lbc have primarily investigated its role in RhoA regulation (38, 42) and the activation of

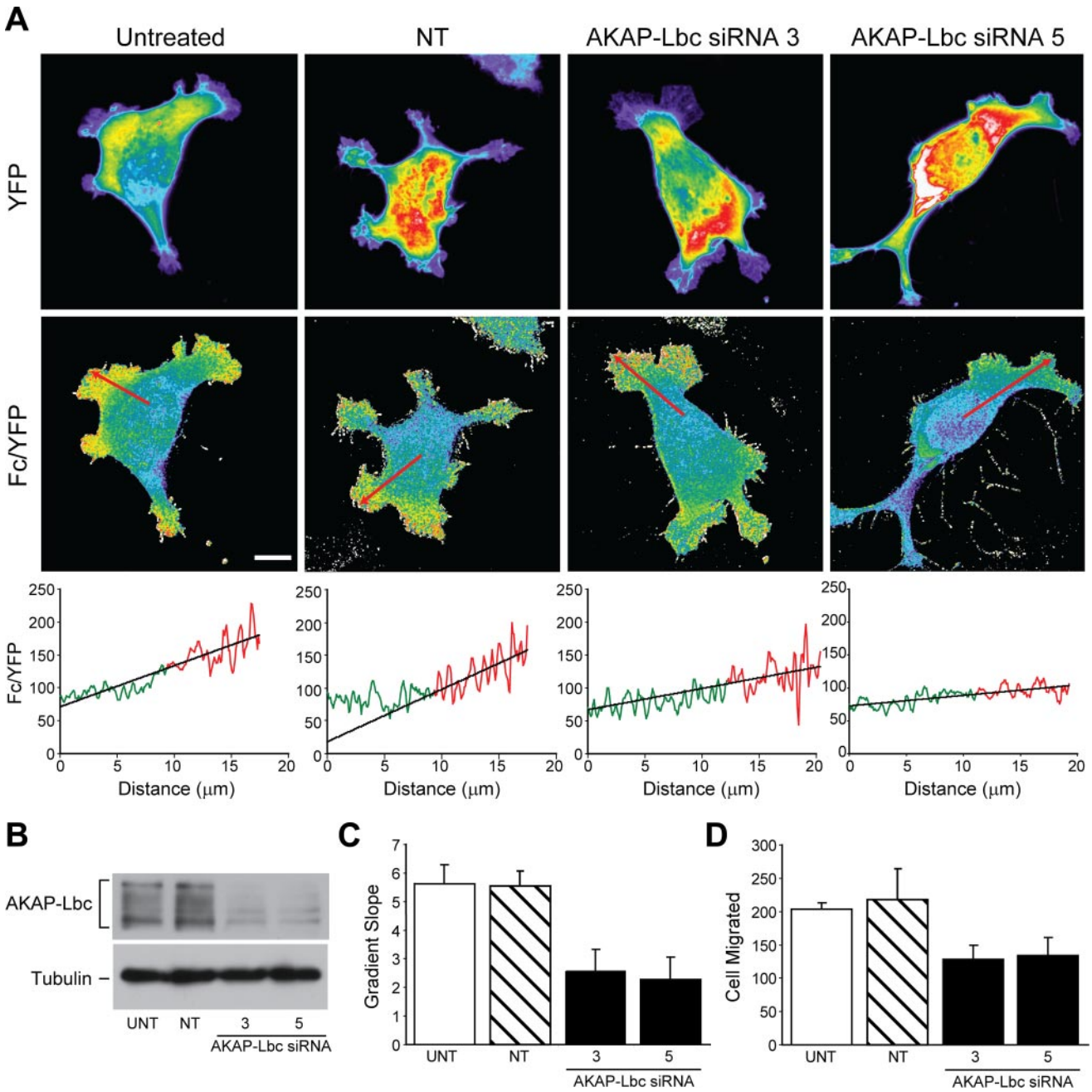

FIGURE 6. **AKAP Lbc is important for the formation of active PKA gradients.** Clone A cells were transfected with AKAR1 only (untreated sample (*UNT*)) or AKAR1 plus non-targeting siRNA (*NT*), AKAP-Lbc siRNA 3 or AKAP-Lbc siRNA 5. After 48 h cells were plated on laminin-1-coated coverslips and allowed to adhere and migrate before they were fixed and imaged as described in Fig. 1. Representative YFP and Fc/YFP images for each condition are shown in *A*. Graphics below the Fc/YFP images represent the average pixel intensity of the Fc/YFP ratio *versus* the distance in microns. Data points in *red* indicate data (8 μm before the edge of the cell) used to determine the slope of the line plot. *B*, immunoblotting assay was performed on untreated cells or cells electroporated with NT, AKAP-Lbc 3, or AKAP-Lbc 5 siRNAs; representative data showing siRNA-mediated knockdown of AKAP-Lbc expression are shown. *C*, the slopes taken from multiple cells (untreated, $n = 20$; NT siRNA, $n = 19$; AKAP-Lbc siRNA 3, $n = 11$; AKAP-Lbc siRNA 5, $n = 9$) were averaged and graphed in the histogram representing the means ± S.E. p value for untreated sample *versus* either AKAP-Lbc siRNA 3 or 5 = 0.003. There was no statistical difference between the UNT and NT siRNA-treated cells. *D*, Transwell haptotactic migration assay were performed with Clone A cells that were electroporated only or transfected with non-targeting siRNA, AKAP-Lbc siRNA 3, or AKAP-Lbc siRNA 5 as described under "Experimental Procedures." Statistical analysis revealed that both individual AKAP-Lbc siRNAs reduced haptotactic migration significantly (p value = 0.01 and 0.03, respectively) compared with either untreated cells. No statistical difference was noted between the untreated and NT siRNA-treated cells.

other protein kinase cascades (43). The role of its AKAP function in this context involves the negative feedback regulation of RhoA where PKA phosphorylation of AKAP-Lbc blocks its guanine nucleotide exchange factor function through the mobilization of a 14-3-3-dependent pathway (44, 45). We find that AKAP-Lbc does not appear to function as a Rho guanine nucleotide exchange factor in unstimulated Clone A cells in response to laminin binding[4] despite the fact that Clone A cells activate and require RhoA during laminin-1-mediated migra-

[4] A. A. Paulucci-Holthauzen, M. Chen, and K. L. O'Connor, unpublished observation.

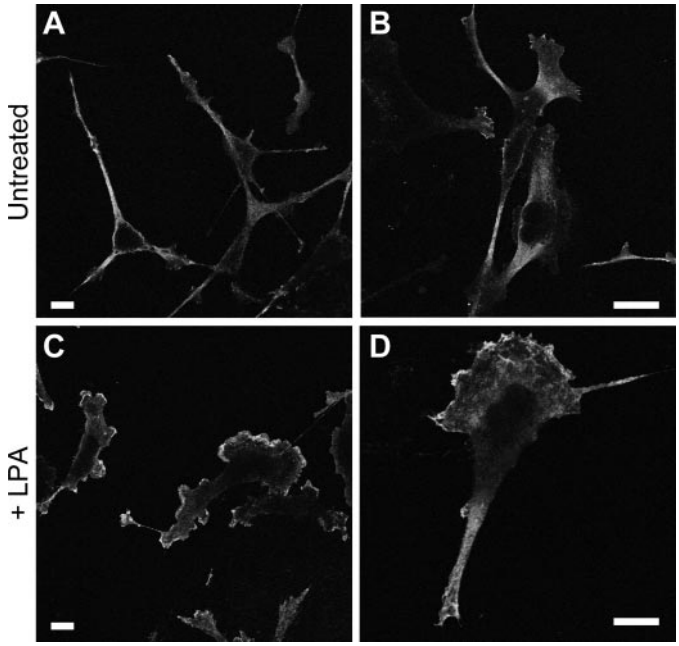

FIGURE 7. **LPA-stimulated MDA-MB-231 cells display high PKA activity at the leading edge.** MDA-MB-231 cells were plated on collagen-coated coverslips and then left untreated (*A* and *B*) or treated with 100 nM LPA for 15 min (*C* and *D*). Cells were then immunostained for phospho-PKA substrates as described under "Experimental Procedures." Representative confocal images for each condition are shown at two different magnifications. The *bar* in each *panel* indicates 10 μm.

tion (26). Therefore, we postulate that the role of AKAP-Lbc in cell migration in the current study is mediated primarily through its kinase anchoring function rather than its guanine nucleotide exchange factor functions. This finding is consistent with another role of this anchoring protein in the heart, where its kinase anchoring function predominates over guanine nucleotide exchange factor activity in the coordination of signaling events that regulate the onset of cardiac hypertrophy (46). We further suggest that AKAP-Lbc serves to couple PKA to other PKA targets relevant to cell migration. AKAP-Lbc ablation does not, however, completely obliterate PKA activity gradients in the manner of the Ht31 peptide. This suggests that other AKAPs may also contribute to localized PKA activity during cell migration. Other candidate AKAPs include WAVE-1 and Ezrin. WAVE-1 is a major actin cytoskeleton-associated AKAP (47) that is recognized to play a critical role in cell migration through actin cytoskeletal rearrangement. Specifically, WAVE-1 acts as the molecular scaffold to couple the Arp2/3 complex and Rac1 small GTPase to the formation of the actin meshwork within lamellae (48). Ezrin is a membrane-associated AKAP also recognized as a mediator of cell migration through its functions at the leading edge (49, 50). Yotiao is also a viable candidate, as it is found on the plasma membrane where it is recognized to influence ion channel activity (14). Future studies are needed to determine what other AKAPs may be involved in PKA activity gradient formation and mechanistically how they contribute specifically to the spatial events that control cell motility.

An interesting finding of our study is that PDE activity is not involved in the formation of PKA activity gradients but, rather, is critical for restricting where these gradients can form. We find that cells that are migrating display PKA activity gradients that are restricted to the leading edge of the cell and within the lamellae. Under conditions where PDEs are inhibited and basal PKA activity levels are elevated, PKA activity gradients are no longer polarized yet still form most likely due to the diffusion of cAMP away from the plasma membrane. Because PKA is understood to control key signaling events at the leading edge, the disruption of this polarization of PKA gradients would cause a loss of directionality and, thus, impede cell migration. This concept is supported by previous studies on the essential role of PDEs during cell polarization and migration (5, 26, 32). This observation is contradictory to the proposed role of PDEs in gradient formation based on computer modeling (51) and experimental models showing that PDEs restrict cAMP diffusion (15, 52); however, it is supported by other studies that demonstrate that PDEs are essential to restrict cAMP/PKA signaling spatially (53–55). PDEs are known to be either cytosolic or anchored to other molecules such as AKAPs (14, 31). The co-distribution of both enzyme classes underscores the transient nature of the cAMP response. Type 4 PDEs, which can specifically degrade cAMP, have been reported to bind several different AKAPs (14, 16). Furthermore, adenylyl cyclases have been shown to be dynamically regulated by associated AKAPs as recently shown with adenylyl cyclase V/VI (56). If select AKAPs can serve as molecular scaffolds to bring together PDEs and adenylyl cyclases, the presence of the PDEs at the site of cAMP generation could influence the threshold of cAMP generation needed to activate PKA, lead to a PKA activity gradient, and thus, influence the polarization process. Deciphering exactly how PDEs contribute to PKA activity compartmentalization and gradient formation will certainly require further study.

Although we interpret our results throughout our study as evidence of PKA activity gradients, the AKAR1 FRET reporter construct actually reports the lifetime of a single phosphate which is initiated by PKA and terminated by a phosphatase. Ultimately, it is the phosphate attached by PKA that mediates the signaling events downstream of PKA. We and others have implicated PKA as a critical kinase during directed migration through the phosphorylation of select substrates (6–9). How this is balanced by its phosphatase counterpart during cell migration is not understood. Interestingly AKAPs are known to anchor phosphatases as well as kinases (14). It is an intriguing concept that select AKAPs could serve as focal points for initiation and termination of the phosphorylation of PKA substrates through its kinase and phosphatase anchoring, respectively, to keep PKA signaling transient. How phosphatases impact this system will be an important topic for future studies.

Together with previous observations regarding the role of PKA activity in cell migration, we propose the following model. During cell migration, *de novo* engagement and clustering of β1 integrins occurs at the leading edge. Upon integrin engagement, adenylyl cyclases are stimulated (40). Then PKA anchored to select AKAPs, such as AKAP-Lbc as shown here, in close proximity to integrin complexes (41), and the associated actin cytoskeleton is activated. Because of its transient nature (6), this PKA activation through integrin ligation is restricted to the leading edge. The polarization of PKA activity is controlled

through the localized excitation of adenylyl cyclases and anchored PKA near integrin receptors, and through the global inhibition of PKA controlled through the degradation of cAMP by PDEs. This idea of the global inhibition and local excitation of PKA would be similar to phosphoinositol triphosphate gradients that are required for chemoattractant gradient sensing in *Dictyostelium* and neutrophils (57). This localized PKA activity would then exert its effects on distinct targets. An example of such a target is RhoA, which is inhibitable by PKA (26, 58–60). In Clone A cells (26) as well as other cells of epithelial origin (61–63), RhoA localizes on the plasma membrane of nascent lamellipodia during cell migration (26, 63), where it is understood to be activated (64). This localization is distinct from that noted for PKA activity, suggesting that PKA and RhoA activities are spatially separated at the leading edge, which would help to restrict the actions of RhoA. Although all modes of cell migration may not require each of these signaling intermediates, other candidates for PKA regulation at the leading edge include cdc42, Rac, PTP-PEST, Csk, Rap1, myosin light chain, and VASP-Abl complexes (for a review, see Ref. 8). The proper localization and actions of these proteins would then allow for the formation of actin cytoskeletal structure that is required for actin-mediated cell protrusions and stabilization of lamellae. Two recent studies have implicated PKA in the activation of the phosphatidylinositol 3-kinase (PI3K) pathway, suggesting that PKA may actually set up the polarization of PI3K activity at the leading edge to facilitate directional migration (33, 65) As a result, we suggest that PKA activity represents one of several complementing ways to distinguish the leading edge from the rest of the cell, a process that is required for directed cell migration (1).

In summary, our study demonstrates the existence of PKA activity gradients in migrating cells and that these PKA activity gradients are mediated by the coordinated actions of cAMP synthesis and PKA anchoring through specific AKAPs such as AKAP-Lbc, whereas PDE activity is important for the polarization of these gradients.

Acknowledgments—We gratefully acknowledge Drs. Jin Zhang and Steve Akiyama for reagents, Drs. Xiaodong Cheng, Sarita Sastry, Don Senger, Min Chen, Luis M. F. Holthauzen, and Wenhong Zhou for helpful discussions, Dr. Heidi Weiss for statistical analysis, Karen Martin for graphics preparation, and L. Nicole Towers and Anusha Srinivasan for technical assistance.

REFERENCES

1. Lauffenburger, D. A., and Horwitz, A. F. (1996) *Cell* **84,** 359–369
2. Meinkoth, J. L., Alberts, A. S., Went, W., Fantozzi, D., Taylor, S. S., Hagiwara, M., Montminy, M., and Feramisco, J. R. (1993) *Mol. Cell. Biochem.* **127–8,** 179–186
3. Taylor, S., Knighton, D. R., Zheng, J., TenEyck, L. F., and Sowadski, J. M. (1992) *Faraday Discuss.* **93,** 143–153
4. Iyengar, R. (1996) *Science* **271,** 461–463
5. O'Connor, K. L., Shaw, L. M., and Mercurio, A. M. (1998) *J. Cell Biol.* **143,** 1749–1760
6. O'Connor, K. L., and Mercurio, A. M. (2001) *J. Biol. Chem.* **276,** 47895–47900
7. Howe, A. K., Baldor, L. C., and Hogan, B. P. (2005) *Proc. Natl. Acad. Sci. U. S. A.* **102,** 14320–14325
8. Howe, A. K. (2004) *Biochim. Biophys. Acta* **1692,** 159–174
9. Goldfinger, L. E., Han, J., Kiosses, W. B., Howe, A. K., and Ginsberg, M. H. (2003) *J. Cell Biol.* **162,** 731–741
10. Corbin, J. D., Sugden, P. H., Lincoln, T. M., and Keely, S. L. (1977) *J. Biol. Chem.* **252,** 3854–3861
11. Hayes, J. S., and Brunton, L. L. (1982) *J. Cyclic Nucleotide Res.* **8,** 1–16
12. Jurevicius, J., and Fischmeister, R. (1996) *Proc. Natl. Acad. Sci. U. S. A.* **93,** 296–299
13. Rich, T. C., Fagan, K. A., Tse, T. E., Schaack, J., Cooper, D. M., and Karpen, J. W. (2001) *Proc. Natl. Acad. Sci. U. S. A.* **98,** 13049–13054
14. Wong, W., and Scott, J. D. (2004) *Nat. Rev. Mol. Cell Biol.* **5,** 959–970
15. Zaccolo, M., Magalhaes, P., and Pozzan, T. (2002) *Curr. Opin. Cell Biol.* **14,** 160–166
16. Dodge, K. L., Khouangsathiene, S., Kapiloff, M. S., Mouton, R., Hill, E. V., Houslay, M. D., Langeberg, L. K., and Scott, J. D. (2001) *EMBO J.* **20,** 1921–1930
17. Taskén, K. A., Collas, P., Kemmner, W. A., Witczak, O., Conti, M., and Taskén, K. (2001) *J. Biol. Chem.* **276,** 21999–22002
18. Zhang, J., Ma, Y., Taylor, S. S., and Tsien, R. Y. (2001) *Proc. Natl. Acad. Sci. U. S. A.* **98,** 14997–15002
19. van Rheenen, J., Langeslag, M., and Jalink, K. (2004) *Biophys. J.* **86,** 2517–2529
20. Gordon, G. W., Berry, G., Liang, X. H., Levine, B., and Herman, B. (1998) *Biophys. J.* **74,** 2702–2713
21. Youvan, D. C., Coleman, W. J., Silva, C. M., Petersen, J., Bylina, E. J., and Yang, M. M. (1997) *Biotechnology et alia* **1,** 1–16
22. Tron, L., Szollosi, J., Damjanovich, S., Helliwell, S. H., Arndt-Jovin, D. J., and Jovin, T. M. (1984) *Biophys. J.* **45,** 939–946
23. Zal, T., and Gascoigne, N. R. (2004) *Biophys. J.* **86,** 3923–3939
24. Paulucci-Holthauzen, A. A., and O'Connor, K. L. (2006) *Anal. Biochem.* **355,** 175–182
25. Chen, M., and O'Connor, K. L. (2005) *Oncogene* **24,** 5125–5130
26. O'Connor, K. L., Nguyen, B.-K., and Mercurio, A. M. (2000) *J. Cell Biol.* **148,** 253–258
27. Rabinovitz, I., and Mercurio, A. M. (1997) *J. Cell Biol.* **139,** 1873–1884
28. Oliveria, S. F., Gomez, L. L., and Dell'Acqua, M. L. (2003) *J. Cell Biol.* **160,** 101–112
29. Valentin, G., Verheggen, C., Piolot, T., Neel, H., Coppey-Moisan, M., and Bertrand, E. (2005) *Nat. Methods* **2,** 801
30. Dormond, O., Bezzi, M., Mariotti, A., and Ruegg, C. (2002) *J. Biol. Chem.* **277,** 45838–45846
31. Houslay, M. D., and Adams, D. R. (2003) *Biochem. J.* **370,** 1–18
32. Fleming, Y. M., Frame, M. C., and Houslay, M. D. (2004) *J. Cell Sci.* **117,** 2377–2388
33. Lim, C. J., Kain, K. H., Tkachenko, E., Goldfinger, L. E., Gutierrez, E., Allen, M. D., Groisman, A., Zhang, J., and Ginsberg, M. H. (2008) *Mol. Biol. Cell* **19,** 4930–4941
34. Carr, D. W., Hausken, Z. E., Fraser, I. D., Stofko-Hahn, R. E., and Scott, J. D. (1992) *J. Biol. Chem.* **267,** 13376–13382
35. Westphal, R. S., Tavalin, S. J., Lin, J. W., Alto, N. M., Fraser, I. D., Langeberg, L. K., Sheng, M., and Scott, J. D. (1999) *Science* **285,** 93–96
36. Marx, S. O., Kurokawa, J., Reiken, S., Motoike, H., D'Armiento, J., Marks, A. R., and Kass, R. S. (2002) *Science* **295,** 496–499
37. Borm, B., Requardt, R. P., Herzog, V., and Kirfel, G. (2005) *Exp. Cell Res.* **302,** 83–95
38. Diviani, D., Soderling, J., and Scott, J. D. (2001) *J. Biol. Chem.* **276,** 44247–44257
39. Chen, M., Towers, L. N., and O'Connor, K. L. (2007) *Am. J. Physiol. Cell Physiol.* **292,** 1927–1933
40. Meyer, C. J., Alenghar, F. J., Rim, P., Fong, J. H.-J., Fabray, B., and Ingber, D. E. (2000) *Nat. Cell Biol.* **2,** 666–668
41. Whittard, J. D., and Akiyama, S. K. (2001) *J. Cell Sci.* **114,** 3265–3272
42. Diviani, D., Baisamy, L., and Appert-Collin, A. (2006) *Eur. J. Cell Biol.* **85,** 603–610
43. Carnegie, G. K., Smith, F. D., McConnachie, G., Langeberg, L. K., and Scott, J. D. (2004) *Mol. Cell* **15,** 889–899
44. Diviani, D., Abuin, L., Cotecchia, S., and Pansier, L. (2004) *EMBO J.* **23,** 2811–2820

45. Jin, J., Smith, F. D., Stark, C., Wells, C. D., Fawcett, J. P., Kulkarni, S., Metalnikov, P., O'Donnell, P., Taylor, P., Taylor, L., Sougman, A., Woodgett, J. R., Langeberg, L. K., Scott, J. D., and Pawson, T. (2004) *Curr. Biol.* **14,** 1436–1450
46. Carnegie, G. K., Soughayer, J., Smith, F. D., Pedroja, B. S., Zhang, F., Diviani, D., Bristow, M. R., Kunkel, M. T., Newton, A. C., Langeberg, L. K., and Scott, J. D. (2008) *Mol. Cell* **32,** 169–179
47. Westphal, R. S., Soderling, S. H., Alto, N. M., Langeberg, L. K., and Scott, J. D. (2000) *EMBO J.* **19,** 4589–4600
48. Takenawa, T., and Miki, H. (2001) *J. Cell Sci.* **114,** 1801–1809
49. Prag, S., Parsons, M., Keppler, M. D., Ameer-Beg, S. M., Barber, P., Hunt, J., Beavil, A. J., Calvert, R., Arpin, M., Vojnovic, B., and Ng, T. (2007) *Mol. Biol. Cell* **18,** 2935–2948
50. Niggli, V., and Rossy, J. (2008) *Int. J. Biochem. Cell Biol.* **40,** 344–349
51. Saucerman, J. J., Zhang, J., Martin, J. C., Peng, L. X., Stenbit, A. E., Tsien, R. Y., and McCulloch, A. D. (2006) *Proc. Natl. Acad. Sci. U. S. A.* **103,** 12923–12928
52. Zaccolo, M., and Pozzan, T. (2002) *Science* **295,** 1711–1715
53. Rich, T. C., Fagan, K. A., Nakata, H., Schaack, J., Cooper, D. M., and Karpen, J. W. (2000) *J. Gen. Physiol.* **116,** 147–161
54. Sayner, S. L., Alexeyev, M., Dessauer, C. W., and Stevens, T. (2006) *Circ. Res.* **98,** 675–681
55. Iancu, R. V., Jones, S. W., and Harvey, R. D. (2007) *Biophys. J.* **92,** 3317–3331
56. Bauman, A. L., Soughayer, J., Nguyen, B. T., Willoughby, D., Carnegie, G. K., Wong, W., Hoshi, N., Langeberg, L. K., Cooper, D. M., Dessauer, C. W., and Scott, J. D. (2006) *Mol. Cell* **23,** 925–931
57. Devreotes, P., and Janetopoulos, C. (2003) *J. Biol. Chem.* **278,** 20445–20448
58. Lang, P., Gesbert, F., Delespine-Carmagnat, M., Stancou, R., Pouchelet, M., and Bertoglio, J. (1996) *EMBO J.* **15,** 510–519
59. Laudanna, C., Campbell, J. M., and Butcher, E. C. (1997) *J. Biol. Chem.* **272,** 24141–24144
60. Dong, J.-M., Leung, T., Manser, E., and Lim, L. (1998) *J. Biol. Chem.* **273,** 22554–22562
61. Fukata, Y., Oshiro, N., Kinoshita, N., Kawano, Y., Matsuoka, Y., Bennett, V., Matsuura, Y., and Kaibuchi, K. (1999) *J. Cell Biol.* **145,** 347–361
62. Nishiyama, T., Sasaki, T., Takaishi, K., Kato, M., Yaku, H., Araki, K., Matsuura, Y., and Takai, Y. (1994) *Mol. Cell. Biol.* **14,** 2247–2456
63. Kurokawa, K., and Matsuda, M. (2005) *Mol. Cell. Biol.* **16,** 4294–4303
64. Bokoch, G. M., Bohl, B. P., and Chuang, T.-H. (1994) *J. Biol. Chem.* **269,** 31674–31679
65. Deming, P. B., Campbell, S. L., Baldor, L. C., and Howe, A. K. (2008) *J. Biol. Chem.* **283,** 35199–35211